OPEN ACCESS
IOP Publishing | Bureau International des Poids et Mesures Metrologia
Metrologia **62** (2025) 035003 (8pp) https://doi.org/10.1088/1681-7575/adcd7b

Advancements in the NRC-FCs2 primary frequency standard

Scott Beattie[1,*], Bin Jian[1], Claude Marceau[1], Kurt Gibble[2] and Marina Gertsvolf[1]

[1] National Research Council Canada, Ottawa, ON K1A 0R6, Canada
[2] Department of Physics, The Pennsylvania State University, University Park, PA 16802, United States of America

E-mail: Scott.Beattie@nrc-cnrc.gc.ca

Received 20 November 2024, revised 11 April 2025
Accepted for publication 16 April 2025
Published 2 May 2025

Abstract

We have made improvements in the stability, accuracy, and performance of the NRC-FCs2 fountain clock. The dominant systematic effects have been re-evaluated. Optically-stabilized microwaves are used to improve the short-term stability, now reaching $\sigma_y = 3 \times 10^{-14}\,\tau^{-\frac{1}{2}}$. We have evaluated the distributed cavity phase shift using absorption imaging. This technique dramatically reduces the evaluation time and final uncertainty. We have re-evaluated biases due to microwave leakage and synchronous phase transients with higher accuracy. The total systematic uncertainty of NRC-FCs2 is now 1.1×10^{-16} in fractional frequency, a factor of 2 improvement over its most recent evaluation.

Keywords: primary frequency standard, atomic clock, SI second, atomic fountain clock, frequency metrology

1. Introduction

Cesium fountain clocks provide the most accurate realization of the SI second and constitute the largest contribution in the steering of International Atomic Time (TAI) [1]. The SI second underpins the metric system, as all base units, excepting the mole, include the second in their definitions.

In recent years, the improvement of optical frequency standards has vastly outpaced that of cesium fountain clocks. Due to their high transition frequencies, the most precise optical clocks now report systematic uncertainties at the level of 10^{-18} and below [2–7], two orders of magnitude better than the most accurate fountain clocks. This has motivated work to prepare for a redefinition of the SI second, which is currently limited by the accuracy achievable by cesium microwave standards.

Although the next definition of the SI second is yet undecided, a roadmap towards the redefinition has been established, with several mandatory criteria [8]. One such criterion requires high-accuracy absolute frequency measurements of optical clock transitions, necessitating comparisons against fountain clocks. This requirement ensures continuity for the transition to a future definition of the second.

Absolute optical clock frequency measurements must achieve a total uncertainty below 3.0×10^{-16} to be included in the calculation of accepted transition frequencies by the International Bureau of Weights and Measures (BIPM). This is challenging, as these measurements are limited by the cesium standards involved, which operate with systematic uncertainties near or above this value [9]. Consequently, improvements to Cs fountains directly enhance the current realization of the SI second and also support a future redefinition of the SI second through absolute measurements of optical frequencies.

Here, we describe improvements made to the operation and evaluation of the NRC-FCs2 fountain clock that have resulted in a significant reduction of its total systematic uncertainty.

* Author to whom any correspondence should be addressed.

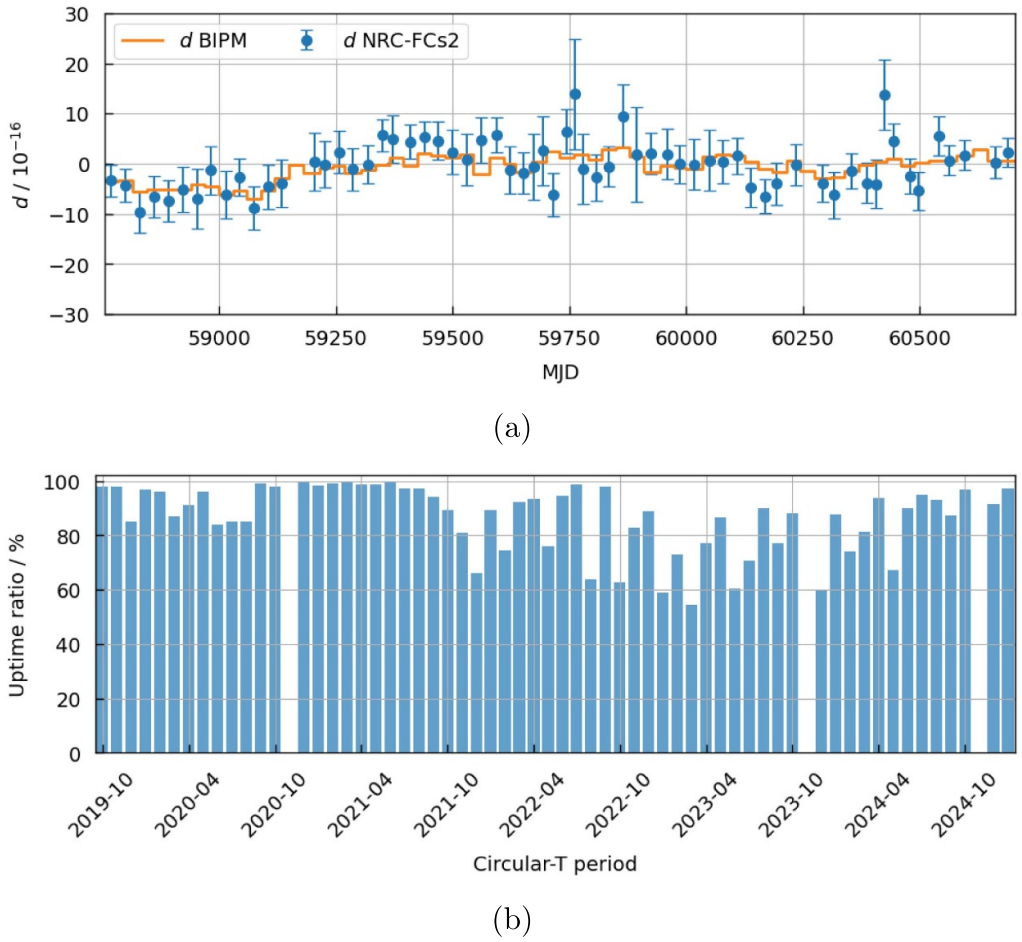

Figure 1. Performance of the NRC-FCs2 fountain clock from October 2019 to January 2025. (a) The blue data points show the fractional frequency difference, d, between NRC-FCs2 and the scale interval of TAI. The orange line denotes the BIPM's estimate of d based on a weighted average of all primary and secondary frequency standards contributing to the steering of TAI. (b) Uptime of the NRC-FCs2 primary frequency standard.

2. NRC-FCs2 performance and microwave source

Since the NRC-FCs2 fountain clock was first evaluated in 2020 [10], it has operated reliably with an unscheduled down time below 10%. The contributions of the NRC-FCs2 fountain clock to the steering of TAI through monthly submissions to the BIPM are shown in figure 1. From October 2019 to January 2025, NRC-FCs2 contributed in all but three months, and was in close agreement with other reporting standards. Over this period, the average deviation of NRC-FCs2 from TAI was $0.5(2.9) \times 10^{-16}$.

An optically-referenced ultra-stable microwave local oscillator, added in 2023, has significantly improved the fountain clock operation. The ultra-stable microwaves are generated by locking a fiber-based optical frequency comb to a 4 Hz-wide ultra-stable laser and drift-corrected reference cavity at 674 nm [11], and stabilizing an SDI-Cs1 commercial microwave synthesizer to the comb repetition rate. The stabilized laser light is delivered to the comb via a 110 m noise-cancelled polarization-maintaining fiber. With the comb locked to the narrow-linewidth laser, $57.5 \times f_{\mathrm{rep}} = 9.2$ GHz is mixed with a fixed 9.2 GHz output of the microwave synthesizer, where f_{rep} is the comb repetition rate. This generates an error signal that is used to stabilize the synthesizer to the comb repetition rate. The 9.2 GHz from the synthesizer is produced by a dielectric resonator oscillator (DRO). The DRO is locked to a 100 MHz low-noise oven-controlled crystal oscillator (OCXO), which itself is locked to a 5 MHz OCXO that serves as the base for the internal frequency synthesis chain. The synthesizer is locked to the comb by applying feedback to the internal 5 MHz OCXO via voltage tuning. To compensate for drifts in the ultra-stable optical cavity ($\sim$10 mHz s^{-1}), the probe laser frequency is adjusted using a slow servo loop to lock it to either an active hydrogen maser, or the $^{88}Sr^{+}$ clock. The probe laser frequency adjustment is applied via feedback to an acousto-optic modulator that is also used for fiber noise cancellation.

The ultra-stable microwave local oscillator allows the fountain to achieve a short term stability of $\sigma_y = 3 \times 10^{-14} \tau^{-\frac{1}{2}}$ for high atom number, as shown in figure 2. This yields an order of magnitude improvement in averaging time to reach

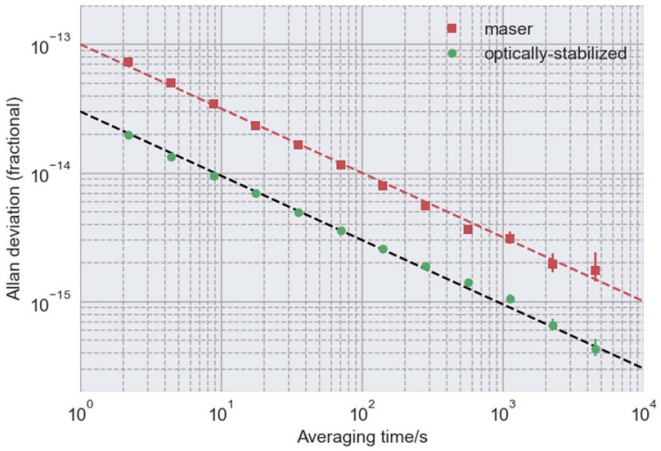

Figure 2. Fractional frequency instability of the fountain. The red squares show the Allan deviation when the local oscillator locked to a hydrogen maser. The dashed red line represents a linear fit to the data which gives $1 \times 10^{-13}\ \tau^{-\frac{1}{2}}$. The short-term stability is improved by more than a factor of three when using optically-stabilized microwaves (green circles). The noise due to the fountain quantum projection and technical noise (based on signal-to-noise ratio measurements) is denoted by the black dashed line, demonstrating that the optically-generated microwaves contributed negligibly to the fountain instability.

the fountain's accuracy compared to that using a hydrogen maser as a frequency reference for the microwave synthesizer, and has facilitated the re-evaluation of several systematic effects. The ultra-stable microwaves are not always available for regular clock operation, but were used to reduce the measurement time for the evaluation of the majority of the systematic effects described in this paper.

3. Systematic shifts

The NRC-FCs2 fountain clock accuracy has been predominantly limited by four effects that have accounted for the majority of the systematic uncertainty: cold collisions, distributed cavity phase (DCP) shifts, microwave leakage, and synchronous phase transients. Here, we describe the re-evaluation of each of these systematic effects.

3.1. Cold collisions

Cesium fountain clocks typically reach atomic cloud temperatures at the level of 1 μK, where cesium atoms have an anomalously large collisional cross-section. Consequently, collisions between laser-cooled atoms can cause a significant systematic bias that scales linearly with density. To characterize the effects of cold collisions, the atomic density of the cloud is varied periodically. The clock's frequency is then extrapolated to zero density for a collisional-shift-free frequency measurement. It should be noted that this method also corrects for any first-order cavity pulling. This shift is typically negligible for cesium fountain clocks. In principle, alternating the atomic density changes much of the uncertainty from systematic to statistical, as it removes density-dependent effects from the extrapolated frequency, but requires longer averaging times. In practice, there is systematic uncertainty from the ratio of atomic densities when they are determined by the ratio of the fluorescence from the number of atoms detected for high and low density. Alternatively, adiabatic rapid passage can accurately prepare atomic density ratios that are a factor of 2 [12]. This technique requires careful pulse shaping and frequency sweeping. Additionally, high/low atom density ratios that are factors of 2 are not optimal for the evaluation of the collisional shift.

For the NRC-FCs2 fountain clock, we toggle between high and low densities to cancel any residual shift by varying the microwave power in the state selection transfer. To determine the uncertainty in the high/low density ratio, we measure the atomic cloud densities directly using absorption imaging. This method is described in [13], where it was shown that the uncertainty in the ratio of densities can easily be below 1%, which results in a typical cold collision systematic uncertainty of 4×10^{-17} for NRC-FCs2, nearly an order of magnitude reduction from that reported in [10].

3.2. Microwave leakage

Atomic fountain clocks are designed to limit the interaction between the cold atom cloud and the interrogating Ramsey microwaves to within the Ramsey cavity. A non-zero microwave field outside of the Ramsey cavity is considered to be microwave leakage, and can cause a frequency bias. In the NRC-FCs2 fountain clock, we have previously observed the effect of leaked microwaves interacting with the atoms below the Ramsey cavity. To address this, the Ramsey cavity microwaves are rapidly detuned by 3 MHz after the atoms descend through the Ramsey cavity using a frequency shift key (FSK) function in the SDI-Cs1 frequency synthesizer. This reduces the effect of the microwave leakage to be below the measurement uncertainty in our previous evaluation of NRC-FCs2, resulting in a shift of $0.1(1.0) \times 10^{-16}$ [10].

To improve on the previous evaluation, we intentionally magnify the effect of microwave leakage by directing amplified microwaves towards the physics package via a microwave horn. The setup is shown in figure 3. Here, the power of the microwaves generated for Ramsey excitation is amplified by over 3 orders of magnitude before being split. In one arm, the microwaves are directed to the Ramsey cavity feeds after attenuation to typical power levels, driving a $\pi/2$ pulse. In the other arm, the amplified microwaves are sent to a microwave horn placed outside the vacuum system, within 40 cm of the microwave cavities. We perform differential measurements with/without the amplified microwaves from the horn and FSK. In these studies, we observe a frequency bias induced by the high-power microwaves of over 2×10^{-12} and a suppression of the bias by a factor of 170 when using FSK to detune the microwave frequency. The effectiveness of FSK in suppressing microwave leakage is most likely

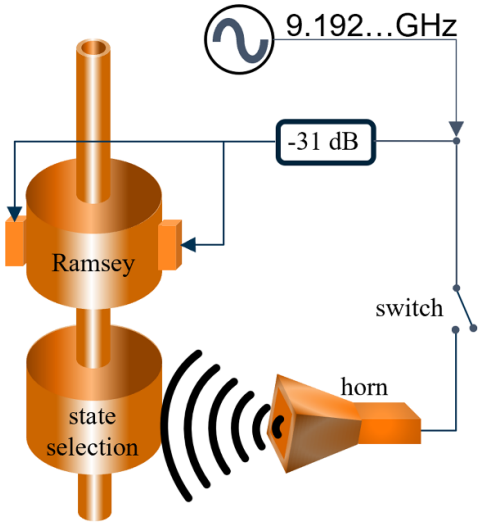

Figure 3. Setup to evaluate microwave leakage. Amplified Ramsey microwaves are split between a microwave horn and the Ramsey cavity feeds. The microwaves directed to the Ramsey cavity are attenuated to their typical power, corresponding to a $\pi/2$ Ramsey pulse. The microwaves pass through a switch, which is used to toggle the 'leakage' microwaves on/off.

limited by the velocity profile of atomic cloud, as the fastest falling atoms will have reached the state selection cavity where leaked microwaves can resonate before the FSK is applied. As the bias due to microwave leakage is $2.5(0.5)\times10^{-15}$ in NRC-FCs2 for normal operation (without FSK), we conclude that FSK suppresses the shift by a factor of 170, to below 2×10^{-17}. We do not correct for the shift, and use 2×10^{-17} as the uncertainty.

3.3. Synchronous phase transients

Atomic fountain clocks operate with a sequence of atomic cooling, launching, interrogation, and detection. Because of this cyclical nature of fountain frequency measurements, equipment that is pulsed will have fixed delays from the Ramsey interrogation time. If this equipment induces a transient phase shift in the local oscillator (microwave synthesizer), it can produce a measurement bias. For example, a difference in phase of 10 µrad on the synthesized 9.192 631 770 GHz between the first and second Ramsey interactions (separated by ∼0.5 s) would result in a measurement bias of over 3×10^{-16}. This is challenging to measure, as there is limited flexibility to vary event timings in order to amplify or reduce this shift. In addition, it is difficult to make a direct phase measurement at the microradian level, which typically requires using an interferometric phase transient analyzer [14].

To re-evaluate the effect of phase transients, we utilize an ultra-stable microwave frequency reference. As described in section 2, by locking a frequency comb to an ultra-stable laser at 674 nm, we produce ultra-stable microwaves based on the comb repetition rate, with a stability better than 1×10^{-14} at 1 s of averaging time. The error signal derived by mixing the microwave synthesizer and comb at 9.2 GHz is described above. It represents a direct measurement of the phase of the synthesized microwaves against the independent and stable reference of the ultra-stable laser. We record the closed-loop error signal for the two Ramsey interaction times and find that there is no systematic phase drift between Ramsey interactions within the statistical measurement uncertainty of 5×10^{-17}. We use this value as the phase transient systematic uncertainty.

This measurement method is insensitive to any phase transients in the final internal mixing stage of the SDI-Cs1 synthesis chain, where a 7.3 MHz signal generated by a direct digital synthesizer (DDS) is mixed with 9.2 GHz from the DRO. It is expected that the phase locks of the internal 5 MHz and 100 MHz OCXOs in the synthesizer would be the most sensitive to any power transients, as the oscillator frequencies are multiplied up by factors of 1840 and 92 in the synthesis chain, respectively. The DDS also detunes the synthesizer frequency via FSK. This is unlikely to introduce significant phase transients as the DDS power is held constant. Additionally, the FSK is applied for a short time immediately after the second Ramsey interaction, allowing the synthesizer ∼0.5s to stabilize before the first Ramsey interaction in the subsequent experimental cycle. It should also be noted that since the previous evaluation of NRC-FCs2 in 2020, the synthesizer used as a local oscillator is now housed in a separate lab from the fountain electronics, optics, and physics package. This location is over 30 m away from any equipment with a cyclical power draw, such as optical shutters, radio frequency amplifiers, or MOT magnetic field coils.

3.4. DCP

The DCP shift arises from variations in the phase of the Ramsey microwaves, for example, due to imbalanced feeding or inhomogeneous cavity wall losses. When the launch of the atomic cloud is not vertical, the horizontal velocity component couples with the phase variations to give an effective Doppler shift. Therefore, to characterize these effects requires knowledge of both the verticality of the atomic launch, as well as the sensitivity of the clock frequency to cloud displacements in the Ramsey cavity.

It has been shown in [15, 16] that it is useful to represent the Ramsey cavity microwave field as a Fourier expansion of azimuthal terms $g_m(r,z)\cos m\phi$, where m is an integer, ϕ is the azimuthal angle, and r and z are the radial and longitudinal coordinates, respectively. It is sufficient to consider only the lowest 3 modes ($m\leqslant2$), of which $m=1$, corresponding to power flow across the cavity, contributes the largest uncertainty in NRC-FCs2.

The most common method to evaluate and minimize the $m=1$ DCP shift is to vertically align the fountain by using the shift itself as a tilt sensor. In this case, the DCP shift is enhanced by feeding the Ramsey cavity asymmetrically using only one feed at a time, alternating the feed direction. The fountain is then tilted, and verticality is determined by the

angle where there is no frequency difference when feeding the cavity from opposing directions. The dependence of the clock frequency on launch angle with balanced feeds is then measured. This frequency sensitivity to tilt, combined with the tilt and its uncertainty, yields an $m = 1$ DCP bias and uncertainty.

This method is effective, however, it is also time-consuming. These measurements are typically not automated, and changing the tilt angle generally requires human intervention. For these reasons, it is common to carefully characterize the fountain alignment during a full systematic evaluation, but not to make regular measurements of the atomic trajectory, which can change over time. Another issue with the technique, is that it requires using the DCP shift itself as a sensor. In NRC-FCs2 (and other fountains), the Ramsey cavity has been designed with the intention of having a low DCP shift. This makes it difficult to realize a precise vertical alignment using this method.

An alternate technique to evaluate $m = 1$ DCP shifts applies a small and variable magnetic field transverse to the C-field to locate the Ramsey cavity crossing positions [17]. This technique yields uncertainties due to DCP well below 1×10^{-16}, but requires that conductors/coils be placed inside of the magnetic shielding. Here, we instead use absorption imaging, as described in [13], to directly measure the trajectory of the atomic cloud in the fountain. Using this method, full information of the trajectory of the atomic cloud can be obtained within minutes by taking images at a series of ballistic flight times after launch.

To map the trajectory of the atoms, the imaging light is aligned vertically to a high accuracy to minimize conflating a misaligned imaging beam with a horizontal atomic motion. The first step is to establish an accurate vertical reference. For this, the downward trapping beam is split on a non-polarizing beamsplitting cube, with 90% of the light incident on a liquid surface below the physics package and 10% of the light directed towards a retro-reflecting corner-cube, as shown in figure 4(a). To create an optical path to the liquid surface, a mirror used in the upward beam alignment is temporarily removed. The interference pattern formed by the reflected beams from the corner-cube and the liquid surface is then used to measure the verticality of the downward beam. This process allows for precise angular alignment through the relation $\frac{\lambda}{d} = \sin\theta \approx \theta$, where λ is the wavelength, d is the spacing between interference fringes, and θ is the angle between the reflected beams in radians. In this case, the angle between the reflected beams is twice the angular deviation of the downward beam from vertical. It is straightforward to align the downward beam such that there is less than two fringes visible over the 14 mm field of view, corresponding to a deviation from vertical of $<30\,\mu$rad.

Due to the design of the NRC-FCs2 physics package, the upward vertical trapping beam is more convenient to use for imaging than the downward beam, as there is ample room above the physics package for optics and a camera. Consequently, a second alignment step is required where we remove the liquid surface, replace the mirror in the upward beam path, and interfere the upward beam with the reflection of the vertically-aligned downward beam from the corner-cube retro-reflector. We then align the upward beam to be anti-parallel to the downward beam, achieving a vertical alignment precision of the upward beam of $<100\,\mu$rad from vertical. It has been verified that the imaging beam remains aligned for long periods with minimal drift. The drift was monitored by focusing the beam onto a CMOS camera and taking intermittent measurements over a 1 month period. The results are shown in figure 5, where the beam remained aligned to $<80\,\mu$rad. The change in beam alignment shows no systematic drift. The standard deviation of 43 µrad is used as uncertainty of the beam alignment.

We use absorption imaging to measure the atomic cloud position at several times during the ballistic flight, as shown in figure 6, to determine the trajectory and temperature of the atoms. The times of flight typically ranged from 0 ms to 300 ms after launch. At longer times, ballistic expansion causes the cloud to be large and diffuse, leading to high uncertainties in determining the cloud center. It is also important to determine the position of the center of the Ramsey cavity in the images. Here, a microwave excitation with elevated power is applied in the Ramsey cavity and the excited atoms are imaged, as shown

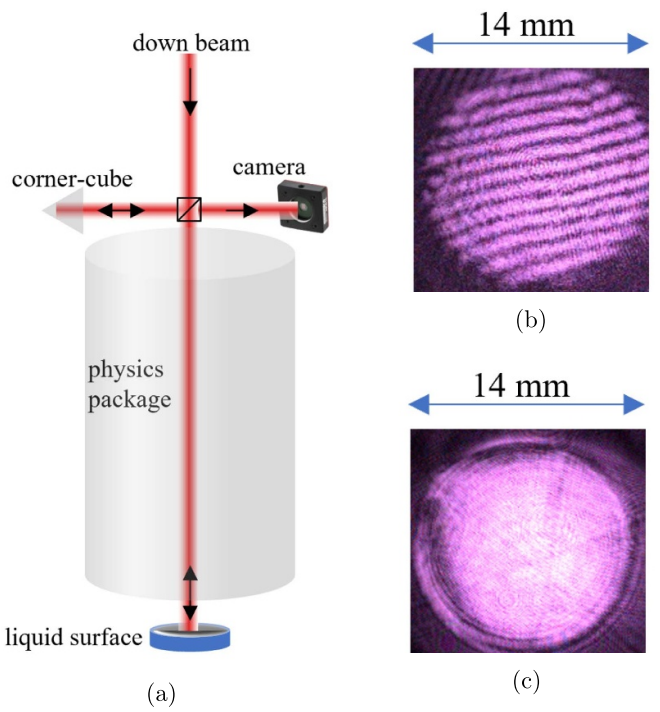

Figure 4. Alignment of the absorption imaging laser beam. (a) The downward cooling beam is split on a non-polarizing beamsplitting cube, with 10% being directed onto a corner-cube retro-reflector and 90% to a liquid surface (vacuum oil) below the physics package. The reflections are recombined on the beamsplitter, and sent to a CMOS camera. (b) The interference pattern when the downward beam is ∼400 µrad from vertical. (c) The interference pattern for a beam aligned to <30 µrad from vertical.

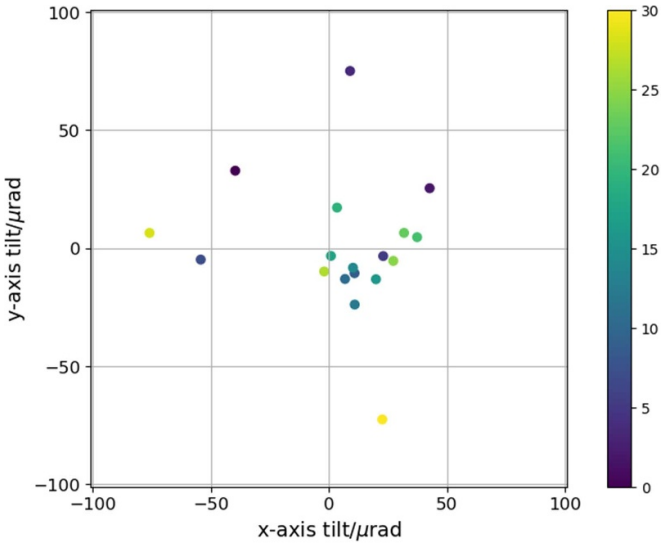

Figure 5. Angular variation of the alignment of the vertical imaging beam over a 1 month period. The colormap denotes the time in days after initial alignment. The beam alignment remained within ±80 μrad of vertical, with a standard deviation of 43 μrad.

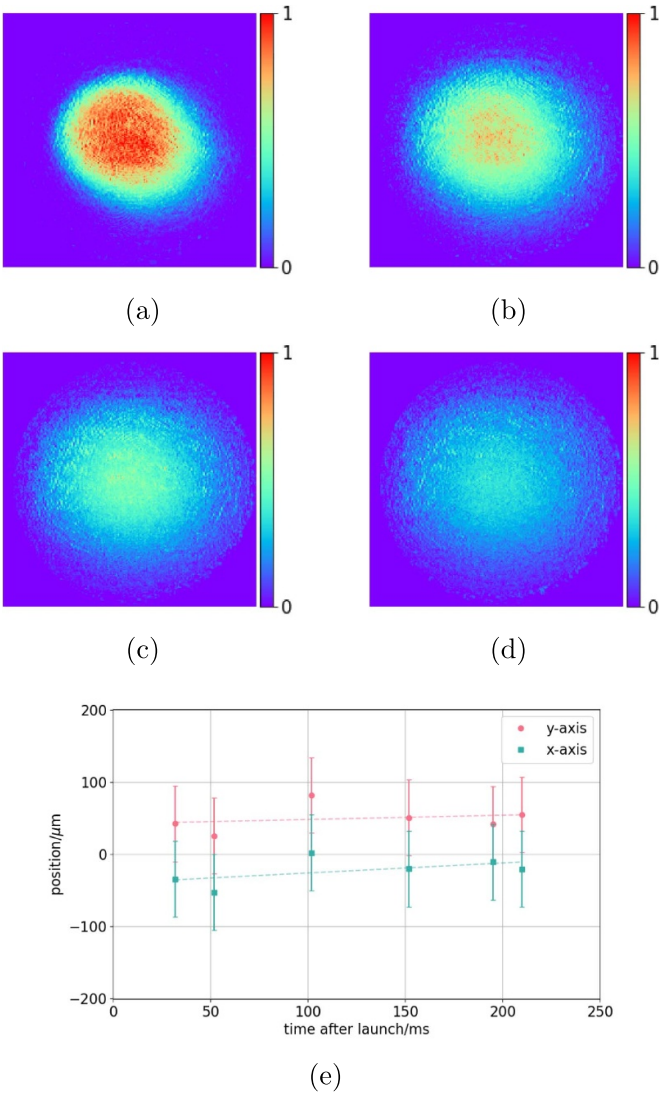

Figure 6. (a)–(d) Absorption images showing the optical density of the atomic cloud 30 ms, 100 ms, 150 ms, and 195 ms after it was launched, respectively. (e) The atomic cloud trajectory based on 2D Gaussian fits to absorption images. For these data, the horizontal launch velocities obtained from linear best fits are 142 μm s^{-1} and 60 μm s^{-1} for the x and y axes, respectively. The vertical launch velocity is 4.3 m s^{-1}. This corresponds to launch tilts of 32(25) μrad and 14(39) μrad from vertical in the x and y directions, respectively.

in figure 7 for a 7π pulse. In this way, the cloud can be aligned within 70 μm of the Ramsey cavity axis and within 100 μrad of vertical.

Ultimately, the quantity of interest is the horizontal displacement of the center-of-mass of the detected atoms in the Ramsey cavity on the cloud's descent, $\mathbf{d}_\mathrm{d}$, with respect to the cavity crossing position on the ballistic ascent, $\mathbf{d}_\mathrm{u}$, which can be expressed as, $\mathbf{d}_\mathrm{ud} = \mathbf{d}_\mathrm{d} - \mathbf{d}_\mathrm{u}$. This can be decomposed into scalar components $d_\mathrm{ud}(\|)$ and $d_\mathrm{ud}(\perp)$ which are the up/down displacement parallel and perpendicular to the cavity feed axis, respectively. A direct measurement of $\mathbf{d}_\mathrm{u}$ is made via imaging, however, $\mathbf{d}_\mathrm{d}$ must be inferred by modelling the atomic trajectory based on the position, velocity, and temperature determined by imaging the first 300 ms of ballistic flight. Immediately after alignment, $|\mathbf{d}_\mathrm{u}|$ and $|\mathbf{d}_\mathrm{d}|$ are less than 70 μm, however, the atomic launch can drift over time due to changes in MOT beam intensities. Over a 23 d period, the drift of the atomic trajectory caused a 125 μm displacement between the cavity crossings on both axes. This is the dominant contribution to the uncertainty of the cavity crossing displacement. As we intend to only repeat the alignment process monthly, we use 200 μm as an estimate of the uncertainty in the magnitude of the cavity crossing displacement along each axis, $\delta d_\mathrm{ud}(\|)$ and $\delta d_\mathrm{ud}(\perp)$.

The sensitivity of the fountain to displacement in cavity crossing positions can be determined through differential measurements with horizontally translated atomic clouds. Two pairs of shim magnetic coils are positioned along and perpendicular to the cavity microwave feeds, and are used to translate the atomic cloud in the MOT by up to ±3.5 mm in each transverse direction. Due to the expansion of the atomic cloud during its ballistic flight and the 14 mm apertures that truncate the cloud, the shift in the center-of-mass of the detected atoms during their descent through the Ramsey cavity is small. Shifting the MOT position results in displacements of $d_\mathrm{ud}(\|)$, $d_\mathrm{ud}(\perp) = \pm 2.3$ mm. Fractional frequency sensitivities measured along ($\|$) and perpendicular ($\perp$) to the cavity feeds were $\delta f_\| / d_\mathrm{ud}(\|) = 1.6\,(1.0) \times 10^{-16}\,\mathrm{mm}^{-1}$ and $\delta f_\perp / d_\mathrm{ud}\,(\perp) = 0.1\,(0.9) \times 10^{-16}\,\mathrm{mm}^{-1}$, respectively, where δf is the measured fractional frequency shift. Combining the uncertainty in δd_ud with the measured sensitivity on both cavity axes yields an overall uncertainty for the $m = 1$ DCP shift of 4×10^{-17} in fractional frequency.

The contributions of the $m = 0$ and $m = 2$ modes of the microwave field are treated as in [10]. For $m = 0$, an asymmetry in cavity endcap surface resistances with an uncertainty of 10% is considered, as well as a 10% difference in the power supplied by the upper and lower sets of feeds of the

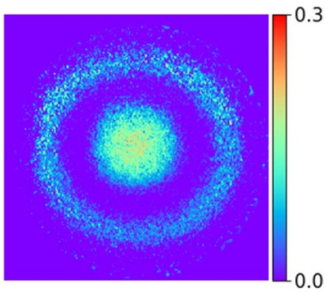

Figure 7. Absorption image of the atom cloud in the center of the Ramsey cavity with elevated microwave power. Here, the Ramsey cavity power corresponds to $\sim 7\pi$ transfer.

Ramsey cavity. The typical atomic cloud radius and temperature are 1.6 mm and 2.0 μK, respectively. This yields a bias of $0.06(34) \times 10^{-16}$ in fractional frequency. The effect of the $m = 2$ mode is calculated based on the spatial uniformity of the atom detection, and the offset of the atomic cloud from the vertical axis. Using 200 μm as a maximum displacement of the atomic cloud from the cavity axis yields a frequency bias of $0.00(2) \times 10^{-16}$.

3.5. Other effects

Several other systematic effects have also been re-evaluated in NRC-FCs2, leading to minor adjustments in the frequency corrections and error budget.

The orthometric height of the fountain lab is increasing at 3 mm yr^{-1} due to post-glacial rebound with respect to the CVGD2013 geoid model [18]. Accordingly, the orthometric height used in calculations of the gravitational redshift of NRC-FCs2 has been adjusted to 91.814(24) m. Although the correction from [10] is well below the uncertainty, the change in height is known, and is therefore applied. Natural Resources Canada have previously surveyed the area and measured local gravity to be 9.80616(1) m s^{-2}. This yields a gravitational redshift of $104.54(3) \times 10^{-16}$. This is a change in the bias at the 10^{-18} level.

The performance of the thermocouples used to determine the temperature of the drift tube has been re-evaluated. The previous calibration of the thermocouples yielded a 0.05 °C uncertainty. The 3 thermocouples are placed along the length of the flight tube, and show a consistent 0.05 °C–0.1 °C variation in readings. We take the average as the temperature for blackbody radiation calculations, and 0.05 °C as the uncertainty in temperature due to potential temperature gradients. This is added in quadrature with the uncertainty in the calibration of the thermocouples to yield a total uncertainty in temperature of 0.07 °C. The shift is then calculated using the equation

$$\frac{f}{f_0} = \beta \left(\frac{T}{300\ \mathrm{K}} \right)^4 \left[1 + \epsilon \left(\frac{T}{300\ \mathrm{K}} \right)^2 \right], \qquad (1)$$

where T is the temperature of the drift tube [19]. We use the blackbody coefficient values $\beta = -1.710(6) \times 10^{-14}$ and $\epsilon = 1.3(1) \times 10^{-2}$ as calculated in [20, 21] respectively. This leads to a shift of $-162.5(6) \times 10^{-16}$ for our typical flight tube temperature of 22.1 °C. The uncertainty in the temperature contributes 0.15×10^{-16}, while the uncertainty due to the numerical coefficients β and ϵ is 0.59×10^{-16}.

Microwave lensing has also been re-evaluated. The shift is calculated as in [10] and described in [22]. For our typical cloud parameters given above, the calculation yields a bias of $0.6(2) \times 10^{-16}$.

The systematic effects of background gas collisions, AC Stark shifts, Rabi pulling, microwave spectral purity, Ramsey pulling, cavity pulling (2nd order), and Majorana transitions have been evaluated to have a contribution below 10^{-17} in fractional frequency [10], and are not listed in table 1.

Table 1. Uncertainty budget of NRC-FCs2 listing the systematic effects, and their associated frequency biases and uncertainties, given in parts in 10^{16}. Here, the re-evaluated biases/uncertainties are applied for the period of modified Julian date 60534–60549, and these data are representative of typical performance.

Systematic effect	Bias	Uncertainty
Zeeman effect	724.4	0.2
Blackbody radiation	−162.49	0.59 (polarizability) 0.15 (temperature)
Gravitational redshift	104.52	0.03
Cold collisions	—	0.39
DCP $m = 0$	0.06	0.34
DCP $m = 1$	0	0.4
DCP $m = 2$	0	0.02
Microwave lensing	0.6	0.2
Microwave leakage	0	0.2
Synchronous phase transients	—	0.5
Total	667.1	1.1

4. Conclusions

The resulting uncertainty budget from the re-evaluation of the NRC-FCs2 fountain clock is given in table 1. The re-evaluation yields an overall systematic uncertainty of 1.1×10^{-16}, a factor of 2 smaller than the most recent evaluation [10]. The largest single contributing uncertainty is the theoretical blackbody coefficients, at 5.9×10^{-17} in fractional frequency. The utilization of absorption imaging has dramatically shortened the measurement time to evaluate DCP shifts, and reduced the uncertainty. It is a broadly applicable technique for any fountain clock with vertical optical access. This allows for a vertical launch alignment to be integrated into regular maintenance, whereas it can be impractical to do so with more time-consuming methods that require tilting the physics package. The improvements in precision will have a direct benefit on absolute frequency measurements of optical clocks at the NRC, as part of

required milestones on the roadmap to a redefinition of the SI second.

Acknowledgment

This material is based in part upon work supported by the United States National Science Foundation under Award No. 2012117 (KG).

ORCID iDs

Scott Beattie https://orcid.org/0000-0003-2056-2871
Bin Jian https://orcid.org/0000-0002-4588-3957
Claude Marceau https://orcid.org/0000-0002-8167-2727
Kurt Gibble https://orcid.org/0000-0003-3652-9638
Marina Gertsvolf https://orcid.org/0000-0002-1188-2104

References

[1] BIPM The BIPM time department database (available at: https://webtai.bipm.org/database/d_plot.html)
[2] Huntemann N, Sanner C, Lipphardt B, Tamm C and Peik E 2016 *Phys. Rev. Lett.* **116** 063001
[3] Brewer S M, Chen J S, Hankin A M, Clements E R, Chou C w, Wineland D J, Hume D B and Leibrandt D R 2019 *Phys. Rev. Lett.* **123** 033201
[4] Tofful A *et al* 2024 *Metrologia* **61** 045001
[5] Ushijima I, Takamoto M, Das M, Ohkubo T and Katori H 2015 *Nat. Photon.* **9** 185–9
[6] Aeppli A, Kim K, Warfield W, Safronova M S and Ye J 2024 *Phys. Rev. Lett.* **133** 023401
[7] McGrew W *et al* 2018 *Nature* **564** 87–90
[8] Dimarcq N *et al* 2024 *Metrologia* **61** 012001
[9] BIPM 2024 *Circular T* **440** (available at: https://webtai.bipm.org/ftp/pub/tai/Circular-T/cirt/cirt.440)
[10] Beattie S, Jian B, Alcock J, Gertsvolf M, Hendricks R, Szymaniec K and Gibble K 2020 *Metrologia* **57** 035010
[11] Dubé P, Madej A, Bernard J and Shiner D A 2009 *Appl. Phys.* B **95** 43–54
[12] Dos Santos F P, Marion H, Bize S, Sortais Y, Clairon A and Salomon C 2002 *Phys. Rev. Lett.* **89** 233004
[13] Beattie S and Jian B 2023 *Metrologia* **60** 045004
[14] Santarelli G *et al* 2009 *IEEE Trans. Ultrason. Ferroelectr. Freq. Control* **56** 1319–26
[15] Li R and Gibble K 2004 *Metrologia* **41** 376
[16] Li R and Gibble K 2010 *Metrologia* **47** 534
[17] Burrows K, Hendricks R J, Szymaniec K, Gibble K, Beattie S and Jian B 2020 *Metrologia* **57** 065003
[18] Véronneau M and Huang J 2016 *Geomatica* **70** 9–19
[19] Itano W, Lewis L L and Wineland D J 1982 *Phys. Rev. A* **25** 1233–5
[20] Beloy K, Safronova U I and Derevianko A 2006 *Phys. Rev. Lett.* **97** 040801
[21] Angstmann E J, Dzuba V A and Flambaum V V 2006 *Phys. Rev. A* **74** 023405
[22] Weyers S, Gerginov V, Kazda M, Rahm J, Lipphardt B, Dobrev G and Gibble K 2018 *Metrologia* **55** 789